Journal of Applied Polymer Science

Durability and Performance of Polystyrene-*b*-Poly(vinylbenzyl trimethylammonium) Diblock Copolymer and Equivalent Blend Anion Exchange Membranes

Melissa A. Vandiver,[1] Benjamin R. Caire,[1] Zach Poskin,[1] Yifan Li,[2] Sönke Seifert,[3] Daniel M. Knauss,[2] Andrew M. Herring,[1] Matthew W. Liberatore[1]

[1]Department of Chemical and Biological Engineering, Colorado School of Mines, Golden, Colorado 80401

[2]Department of Chemistry and Geochemistry, Colorado School of Mines, Golden, Colorado 80401

[3]X-Ray Science Division, Argonne National Laboratory, Argonne, Illinois 60439

Correspondence to: M. W. Liberatore (E-mail: mliberat@mines.edu)

ABSTRACT: Anion exchange membranes (AEM) are solid polymer electrolytes that facilitate ion transport in fuel cells. In this study, a polystyrene-*b*-poly(vinylbenzyl trimethylammonium) diblock copolymer was evaluated as potential AEM and compared with the equivalent homopolymer blend. The diblock had a 92% conversion of reactive sites with an IEC of 1.72 ± 0.05 mmol g^{-1}, while the blend had a 43% conversion for an IEC of 0.80 ± 0.03 mmol g^{-1}. At 50°C and 95% relative humidity, the chloride conductivity of the diblock was higher, 24–33 mS cm^{-1}, compared with the blend, 1–6 mS cm^{-1}. The diblock displayed phase separation on the length scale of 100 nm, while the blend displayed microphase separation (~10 μm). Mechanical characterization of films from 40 to 90 microns thick found that elasticity and elongation decreased with the addition of cations to the films. At humidified conditions, water acted as a plasticizer to increase film elasticity and elongation. While the polystyrene-based diblock displayed sufficient ionic conductivity, the films' mechanical properties require improvement, i.e., greater elasticity and strength, before use in fuel cells. © 2014 Wiley Periodicals, Inc. J. Appl. Polym. Sci. **2015**, *132*, 41596.

KEYWORDS: batteries and fuel cells; conducting polymers; copolymers; mechanical properties; membranes

Received 24 July 2014; accepted 11 October 2014

DOI: 10.1002/app.41596

INTRODUCTION

Low temperature fuel cells are promising, clean energy conversion technology for portable applications including automobiles and portable electronics.[1–3] Alkali fuel cells (AFC) were first developed by Bacon in the 1930s and later implemented on the NASA Apollo orbiter spacecraft using pure hydrogen and oxygen.[1–4] Traditional AFCs utilize a liquid potassium hydroxide electrolyte to transport hydroxide ions from cathode to anode. The alkali nature of AFCs allows favorable electrode kinetics with the potential for non-precious medal catalysts and more versatile fuel utilization.[5] Unfortunately, exposure to carbon dioxide in the oxidant stream converts the hydroxide ions in the liquid electrolyte to carbonates that form solid precipitates fouling the electrodes and requiring circulation of the electrolyte to filter out the carbonate solids. The superior power density of proton exchange membrane fuel cells (PEMFC), without requiring a CO_2 free oxidant stream, prevented commercial development of the liquid AFC, allowing PEMFCs to dominate low temperature fuel cell research and development.

PEMFCs employ a solid acidic polymer to transport protons from anode to cathode. PEMs have been researched heavily the past several decades resulting in durable, thin films with high proton conductivity. Commercial development of PEMFCs remains difficult due to the high cathode catalysts cost, performance optimized for hydrogen fuel, and membrane lifetime.[6,7] The limitations of PEMFCs have led recent research to focus on developing a solid polymer anion exchange membrane (AEM) as the electrolyte in AFCs.[8] These AEM fuel cells maintain the kinetic benefit of the alkali system, but tethering of the cation species, often ammonium, guanidinium, or phosphonium, to the polymer backbone prevents the formation of solid precipitates, even if the hydroxide counter-ions are converted to carbonates.[4,8,9] Chemical degradation is a concern with AEMs as both the cation species and polymer backbone are susceptible to attack by hydroxide. For this reason, many AEM polymer chemistries are under investigation, including perfluorinated AEMs that resemble perfluorinated sulfonic acid (PFSAs), polysulfone and polyphenylene based AEMs, and precast films (FEP/ETFE) irradiated to generate cation functionalities grafted on

the polymer.[10–16] Various cation species, including quaternary phosphonium, tertiary sulfonium, and guanidinium based compounds, are being studied for alkali stability.[17] Vinylbenzyl trimethylammonium is the most common AEM cation of study, due to ease of functionalization and adequate alkali stability on short time scales.[17] The mobility of hydroxide ions is lower than protons in acidic systems,[18] making it necessary to use thin membranes to reduce ionic resistance in the cell. The inherent limitations of AEM performance makes the development of thin, mechanically robust films critical to successful application in alkali AEM fuel cells.

Development of high performance, mechanically robust thin films require a combination of suitable polymer chemistry and controlled film processing. The ability of block copolymers to self-assemble into phase-separated morphologies has created great interest in both PEM and AEM development. The phase separation generated in block copolymers allows pathways for ion transport while maintaining mechanical integrity of the film.[19,20] Block copolymers for ion exchange membranes generally consist of a hydrophobic block that provides mechanical durability and prevents extreme swelling and a hydrophilic block of conductive polymer that provides the ionic transport pathway in the film. The chemically dissimilar blocks encourage phase separation in the system, generating polymer morphologies that include spherical, cylindrical, lamellar, and bicontinuous.[21] Polystyrene-based block copolymer AEMs have been synthesized and characterized previously, however the mechanical performance of these membranes is unknown.[22,23] Tsai et al., synthesized polystyrene-block-poly(vinyl benzyl trimethylammonium) membrane at a range of IECs by sequential monomer addition using atom transfer radical polymerization. These polymers had well defined block lengths leading to distinct spherical, cylindrical, and lamellar morphologies that greatly influenced ion conduction through the membrane.[22] The polystyrene (PS) diblock of this study was previously blended with poly(phenylene oxide) and studied with respect to morphology, hydroxide conductivity, and mechanical properties; however dropcast films of the pure diblock were not robust enough to study.[24] Through controlled film casting, pure PS diblock films were fabricated for this study. While transport pathways can be generated by the chemical nature of the diblock, controlled film processing ensures film uniformity that is essential for consistent conductive performance and mechanical durability.

While the majority of current AEM research has focused on the development of stable polymer chemistries with high ionic conductivity, consideration the membrane mechanical properties is also necessary. While PFSA membranes have dominated PEMs due to their high ionic conductivity and suitable chemical and mechanical durability,[7,25] the lifetime of a PEM fuel cell is often defined by mechanical failure of the membrane. Polymer electrolyte fuel cells experience a range of humidity conditions during operation causing the membrane to swell and shrink. At high hydrations, the membrane experiences dimensional swelling, and desorption of water at low humidities causes the membrane to contract, leading to significant stresses.[6,26,27] Humidity cycling causes repeated swelling and contraction of the membrane that can generate pinholes and cracks, which lead to eventual catastrophic mechanical failure. Mechanical durability and membrane lifetime can be gauged by rapid humidity cycling of the membrane to the point of gas crossover[28] or pressurized blister tests that simulate the hygrothermal stress developed in constrained membrane.[29] It is more difficult to predict membrane lifetime from traditional tensile tests, however tensile measurements remain a basis for comparison between polymer systems. Measurement of mechanical properties under different hydration levels and after humidity cycling is critical to development of robust AEMs for long-term use in fuel cells.

In this study, a diblock copolymer of polystyrene-*b*-poly(vinylbenzyl trimethylammonium) was evaluated as a potential AEM for fuel cells, and compared with blend films of commercially available homopolymers. Polymer films were prepared in solution, functionalized, and characterized. Conductivity, morphology, and mechanical properties of the polymer films were investigated at a range of humidity conditions. While the two polymer systems have the same initial chemical composition, significant differences in stability, phase separation, and transport were observed for the block copolymer and blended membranes.

EXPERIMENTAL

Materials

The polystyrene-*b*-poly(vinylbenzyl chloride) (PS-*b*-PVBC) block copolymer was synthesized as previously described[24] with a total molecular weight of 85,700 g mol^{-1} and molecular weight distribution of 1.85. The diblock copolymer was prepared with the composition of 32 wt % PVBC block and 68 wt % PS block.

The homopolymers were purchased from Sigma-Aldrich and used without additional treatment. The PS was in the form of beads with an average M_w of 192,000 g mol^{-1}. The PVBC was a mixture of 3- and 4-isomers and was a powder with an average M_w of 100,000 g mol^{-1}. Homopolymers were mixed to obtain the same weight ratio, PS/PVBC, as the diblock copolymer.

Film Formation

The polymers in a powder form, or beads for PS, were mixed with toluene at a concentration of 0.3 g mL^{-1} in a round bottom flask. The solution was heated at 80°C with magnetic stirring until the polymer was completely dissolved as a homogeneous solution, typically 1 h. The warm solution was pipetted on to a glass substrate and drawn across the substrate with a micrometer adjustable film applicator. The film applicator was drawn at a constant speed between 15 and 90 mm/s using a film coater (MTI Corporation's MSK-AFA-III, Richmond, CA). The solution was allowed to evaporate for about 4 h, after which the dried polymer film was covered with methanol and the edges of the film were peeled from the substrate, using a razor blade until the film released. The gap height of the micrometer adjustable film applicator was used to control film thickness and consistency. Blade heights ranged from 100 to 500 μm and final film thickness ranged from 40 to 90 μm.

Conversion of the polymer films to the conductive form was performed by soaking in 25wt % trimethylamine solution in

water for 2 days. The films were then removed and washed repeatedly with deionized water to remove excess amine. Films were then soaked in 1*M* sodium chloride solution overnight to ensure all anions in the film were chloride. Films were washed repeatedly over a period of 2 days to remove excess salts from the film. Films were stored in bags with a small amount of water due to their brittleness when dry. Some films were left in the neutral form for mechanical comparison; these films were stored in bags with a small amount of methanol to prevent film cracking. Films were tested in the chloride form for mechanical testing, as the rheometer cannot be sealed to prevent exposure to carbon dioxide that would exchange hydroxide ions to carbonate and bicarbonate.

Ion Exchange Capacity

The ion exchange capacity (IEC) of the material was determined by an acid/base titration. Membranes were exchanged to the hydroxide form by soaking the film in 1*M* sodium hydroxide solution for 2 days at room temperature followed by repeated washes to remove excess ions. The hydroxide form of the membranes were then soaked in 1*M* sodium chloride solutions for 48 h and the hydroxide ions in solution were titrated using standardized hydrochloric acid and continuous pH monitoring. Two inflection points were seen on the titration curve of pH vs. titrant volume, the first around a pH of 8 and the second at a pH of 5. The two inflection points suggest the hydroxide ions reacted with atmospheric carbon dioxide to form carbonate and bicarbonate ions in solution. The end point for the titration was defined as the second inflection point to correspond with the equivalent molar quantity of hydroxide ions before conversion.

Due to the possible sensitivity of the quaternary ammonium cations to hydroxide, the IEC was verified by titration of the chloride ions in solution after soaking chloride form membranes in 1M sodium bicarbonate solutions for 48 h. Standardized silver nitrate solution, 0.0235*M*, was used to titrate the membrane solutions with a potassium chromate indicator. The end point for the titration was defined as the point where permanent rust colored precipitates were seen in solution.

Water Uptake

Water uptake (WU) was characterized using a dynamic vapor sorption apparatus (SMS DVS Advantage 1, Allentown, PA). A membrane sample, about 4 mm^2, was placed on a glass weigh plate and the change in mass was measured gravimetrically under different humidity conditions. The WU of the membrane was calculated based on eq. (1).

$$\mathrm{WU} = \frac{m_{\%\mathrm{RH}} - m_{\mathrm{dry}}}{m_{\mathrm{dry}}} \times 100 \quad (1)$$

where $m_{\%RH}$ is the mass of the sample at the given relative humidity and m_{dry} is the mass of the dry sample. The mass of the dry membrane was taken as the measured mass at the end of the initial 4-h drying period. Given the WU at saturated conditions and the known IEC of the membrane, the hydration level, λ, which is the number of waters per cation functional group, can be calculated using eq. (2)

$$\lambda = \frac{\mathrm{WU}}{m(\mathrm{H_2O}) \cdot \mathrm{IEC}} \quad (2)$$

Small Angle X-ray Scattering

Small angle X-ray scattering experiments were performed at the X-ray Sciences Division, beamline 12-ID-B, at the Advanced Photon Source at Argonne National Laboratory. Measurements were taken in a transmission geometry using a Pilatus 2M SAXS detector with an acquisition time of 1 s at a beam energy of 12 keV and incoming X-ray wavelength of 1 Å. The 2D scatter was radially integrated to obtain data of intensity vs. scattering vector *q*. The transmission intensity was normalized to exposure time and flux of the direct beam through the sample. Swelling of the samples prevents absolute thickness measurement so the atomic density cannot be determined *in-situ* and the intensity units become arbitrary. A custom built four-sample oven controlled the humidity and temperature of the samples during scattering experiments.[30,31] Typical experiments contained three membrane samples and one empty compartment so a background pattern could be obtained throughout the scattering experiment. The humidity of the sample environment was controlled using a combination of wet and dry nitrogen that were mixed in a helical mixing tube before entering the sample oven. A humidity probe positioned in the sample oven provided real time humidity readout. Based on the humidity measurement gas flows were adjusted to achieve the desired temperature and humidity condition.

Optical Microscopy

A Thermo Scientific™ Nicolet iN10™ Infrared microscope with a permanently aligned 15× objective lens was used to collect optical images. A reflection electronic light-emitting diode illuminator was the light source. Visual images were captured using a built-in high-resolution 1/3-inch color digital camera (USB2 with 1024 × 768 low noise CCD). A dry membrane sample, about 5 mm^2, was positioned on a glass slide ensuring the sample was flat for even illumination. All images were collected under ambient conditions.

Conductivity

The in-plane conductivities (σ) of the membranes were calculated using electrochemical impedance spectroscopy to measure membrane resistance as given by eq. (3) below.

$$\sigma = \frac{l}{R \cdot w \cdot t} \quad (3)$$

where R is the membrane resistance, l is the distance between the sense electrodes, w is the width of the membrane samples, and t is the thickness of the sample. Impedance spectra were obtained over a frequency range of 1–10^6 Hz using a four-electrode test cell connected to a multi-channel potentiostat (BioLogic VMP3, Knoxville, TN). Measurements were made in an environmental chamber to control sample temperature and humidity (TestEquity Model 1007H, Moorpark, CA). The resistance of the membrane was determined from the low frequency intercept of the Nyquist impedance plot. All samples were in the chloride form and experiments were performed at constant relative humidity of 95%RH, varying temperature from 50 to 90°C.

Mechanical Characterization

Mechanical properties of the films were measured using an ARES G2 rheometer (TA Instruments, New Castle, DE) with a Sentmanat Extension Rheometer (SER) fixture (Xpansion Instruments, Tallmadge, OH).[32] The SER fixture has two counter rotating drums that uniaxially stretch the polymer film suspended between the drums. The separate motor and transducer of the ARES G2 rheometer allows for strain controlled operation during which stress is measured by the rheometer. Polymer films were cut into strips of about 7mm (W) × 20 mm (L) with the length being along the draw direction of the film. During initial testing, the polymer film was adhered to the SER drums at elevated temperature, 130–155°C, using the force convection oven (FCO) of the ARES. After adhesion the temperature of the oven was reduced to 100°C, below this temperature films would release from the drums, and the polymer film was stretched at a Hencky strain rate of 0.01 s^{-1}. The films are stretched to the point of failure, and the stress at failure is defined as the magnitude of the stress applied to the film just before break. The percent elongation is the percent increase in film length. The Young's modulus is a measure of the elastic nature of the film and was determined by the slope of the stress vs. strain curve in the elastic region, the linear region at very low strains. Initial mechanical characterization was performed on the cation functionalized diblock and blend films as well as the neutral precursors.

New SER drums were manufactured with a flat pin secured to the drum surface by screws at the top and bottom. This drum design allowed films to be loaded and stretched at lower temperatures.[33] A thin piece of silicon rubber was added to the inside of the pins to prevent membrane slipping during testing. In ambient air the films were positioned between the pin and the drum surface and the screws were tightened to hold the membrane suspended between the two drums. The cationic diblock and blended films were stretched at a Hencky strain rate of 0.01 s^{-1} at 60°C under dry and humidified, 95% RH, conditions. The 60°C dry conditions were achieved using the FCO airflow prebuilt into the ARES. Humidified, 60°C, conditions were achieved using a combination of dry and wet gas streams supplied to the FCO chamber through a secondary port. Flow of the wet gas stream through two humidity bottles (Fuel Cell Technologies, Albuquerque, NM) in series saturated the wet gas stream. The wet and dry gas streams were controlled with two MKS RS-485 mass flow controllers and the streams were premixed and delivered in a heated line to the FCO chamber. A Vaisala HMT337 humidity probe provided real time humidity feedback to LabView software where the gas flows are controlled.

RESULTS AND DISCUSSION

Ion Exchange Capacity

The ion exchange capacities of the functionalized polymer films were determined by acid/base and Mohr titrations. By acid/base titration the IEC of the PS-*b*-PVBTMA diblock copolymer was 1.72 ± 0.05 mmol/g corresponding to a 92% conversion of the vinylbenzyl chloride sites based on the theoretical maximum IEC of 1.87 mmol/g. Acid/base titration was unsuccessful on the PS/PVBTMA homopolymer blend, the pH of the chloride solution that the hydroxide form film was soaked in did not increase significantly, being just higher than neutral. It is expected that the homopolymer blend suffered degradation upon exposure to hydroxide and the ions were subsequently washed away before titration. All subsequent testing of the polymer films was performed in the chloride form so hydroxide degradation was not a concern.

A Mohr titration of chloride ions was performed on the films to confirm the IEC without hydroxide effects. By chloride titration, the diblock film had a measured IEC of 1.73 ± 0.05 mmol/g, within the error of the IEC determined by acid/base titration, suggesting the diblock is stable in hydroxide (1*M* NaOH for 2 days) compared with the homopolymer blend. The IEC of the homopolymer blend by chloride titration was 0.80 ± 0.03 mmol/g, which corresponds to incomplete, 43%, conversion of the vinylbenzyl chloride groups or loss of cations sites due to instability after conversion.

Functionalization of the PVBC homopolymer with cations results in a water-soluble polymer and it is possible some of PVBTMA would wash out of the film following quaternization. However, the high concentration of the solution used to draw the film is expected to provide adequate entanglement of the polymer chains to prevent loss of the PVBTMA. During functionalization no noticeable turbidity was observed, indicative of polymer dissolution, in the trimethylamine solution or the subsequent wash solutions. In addition, no measurable decrease in dry film weight or thickness was detected after functionalization to the cationic form. Attempts to fully convert the homopolymer blend were made by soaking the films in trimethylamine for 4 and 10 days at ambient conditions and using a pressurized cell at 50°C and 30 bar pressure for 10 days. These attempts did not increase the measured IEC, and even lowered conversion in some cases, suggesting unstable cation attachment or dissolution of the PVBTMA as functionalization is increased. The lower IEC of the blend polymer compared with the diblock will be reflected in the remaining membrane characterization including WU, conductivity, and mechanical performance.

Water Uptake

Water uptake in the cationic diblock and blend films was measured gravimetrically using dynamic vapor sorption. Maximum WU at 60°C was 23.4 ± 0.1% for the diblock and 11.6 ± 0.1% for the homopolymer blend. The lower WU of the blend film reflects the lower IEC of the polymer compared with the diblock. These WUs correspond to λ values of 7.5 ± 0.2 and 8.0 ± 0.3 for the diblock and blend, respectively. The λ values are lower than PEMs (14–22),[34–36] and other AEMs (12–25).[37–39] The relatively low WU of these polymers is likely due to the stiff, hydrophobic nature of the PS in the glassy state at 60°C.

Polymer Morphology

Morphology of the diblock copolymer and homopolymer blend were investigated using small angle X-ray scattering (SAXS) under dry and wet conditions at 60°C (Figure 1). At both dry and wet conditions, the diblock membrane has a peak at q equal to 5.7 × 10^{-3} $Å^{-1}$ corresponding to a d-spacing of 110 nm. Under humidified conditions, the diblock film's scattering has an additional shoulder at q equal to 1.5 × 10^{-2} $Å^{-1}$

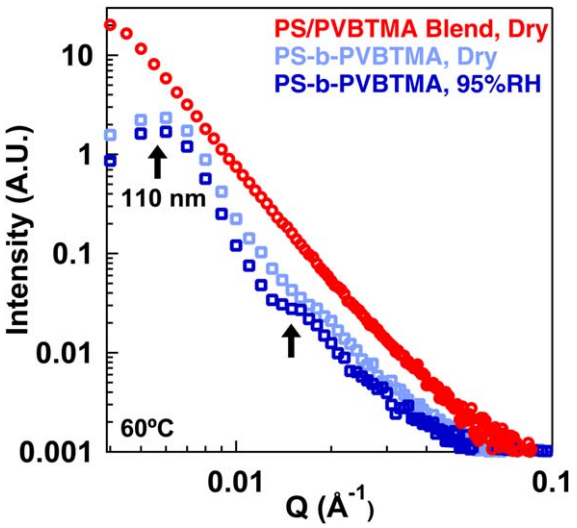

Figure 1. Small angle X-ray scattering patterns for the diblock copolymer membrane under dry (light blue) and humidified (dark blue) conditions and the homopolymer blend membrane under dry conditions (red). The arrows indicate the features of the diblock scattering pattern that correspond to primary *d*-spacing of 110 nm. [Color figure can be viewed in the online issue, which is available at wileyonlinelibrary.com.]

that corresponds to a *d*-spacing of 42 nm. The absence of this shoulder under dry conditions suggests that this size domain is dependent on WU by the polymer. The nanometer scale phase separations of the diblock membrane when humidified will likely facilitate ion conduction through the film. The homopolymer blend film has no features over the SAXS *q*-range because its phase separation is on a much larger length scale.

Optical images of the functionalized diblock and blend membranes were taken at ambient conditions to observe surface morphology and phase separation (Figure 2). The diblock membrane shows no distinguishable characteristics on this micrometer size scale. In contrast, the homopolymer blend membrane has distinct spherical features, indicative of phase separation of the two homopolymers, on the micrometer scale. These spherical regions appear throughout the membrane and range in size between 5 and 50 μm. This scale of phase separation into isolated spherical regions is not favorable for ion conduction, which relies on interconnected pathways through the film. The micrometer scale phase separation that occurs in the homopolymer blend membrane will likely correlate with relatively low ionic conductivity.

Ionic Conductivity

Ionic conductivity of the polymer films in the chloride form were measured at saturated relative humidity and temperatures between 50 and 90°C. The energy of activation for ion conduction was determined over this temperature range using an Arrhenius relationship. Three nominal film thicknesses were tested for both the diblock and homopolymer blend: 40 μm, 70 μm, and 90 μm (Figure 3).

Conductivities were an order of magnitude higher for the diblock copolymer compared with the blend. At 50°C the conductivities of the diblock films were 24–33 mS cm^{-1}, comparable with other AEMs,[4,9,40] while the conductivities of the blend films were only 0.7–6 mS cm^{-1}. The higher conductivity of the diblock compared with the blend is expected due to its higher IEC and nanometer scale phase separation. The conductivities of both the diblock and blend films were highest for the thinnest, 40 μm, films and lowest for the thickest, 90 μm, films. The activation energy for ion conduction was similar, between 15 and 21 kJ mol^{-1}, for both the diblock and blend systems across all thicknesses. These activation energies for ion conduction are similar to other AEMs[15,41] and higher than PFSAs, typically 5–10 kJ mol^{-1}.[15,42] The higher conductivity of the diblock copolymer is a result of its higher IEC as well as more favorable morphology (discussed earlier) for ion conduction compared with the homopolymer blend film. The increased conductivity of thin, diblock films highlights the importance of reducing film thickness while maintaining integrity and ensuring interconnected pathways for ion conduction.

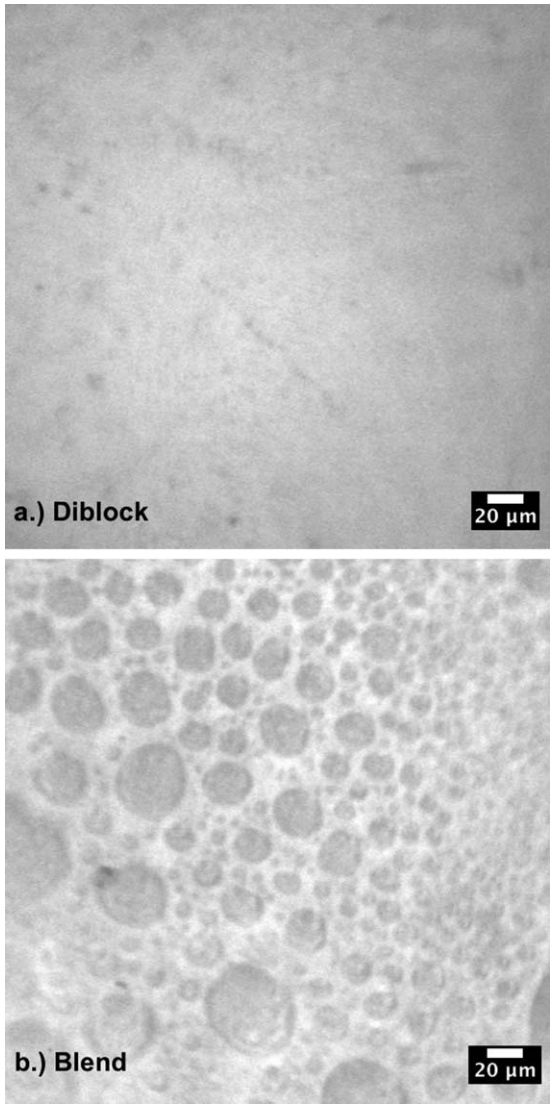

Figure 2. Optical microscope images of the (a) diblock copolymer membrane and (b) the homopolymer blend membrane. The homopolymer blend has isolated regions ranging between 5 and 50 μm.

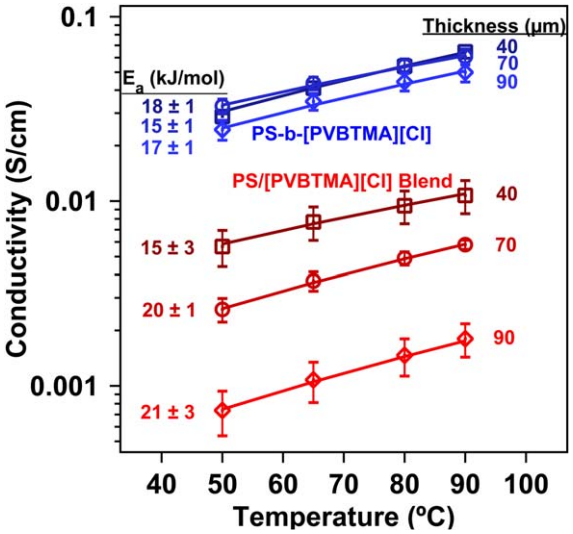

Figure 3. Chloride conductivity of the diblock, PS-*b*-PVBTMA[Cl], shown in blue and the homopolymer blend, PS/PVBTMA[Cl], shown in red. The darkest of each color corresponds with the thinnest, 40 μm, films transitioning to the lightest colors corresponding to the thickest, 90 μm, films. Lines show Arrhenius fits leading to the activation energies listed on the left side of the figure. [Color figure can be viewed in the online issue, which is available at wileyonlinelibrary.com.]

Mechanical Properties

The mechanical properties of the diblock and blended films in both neutral and cationic forms were evaluated by stretching the films to their breaking point at 100°C, under dry air flow. Typical stress–strain curves (Figure 4) allow the determination of stress at break, percent elongation, and Young's (elastic) modulus. Films were tested at same nominal thicknesses (40 μm, 70 μm, and 90 μm) as the conductivity measurements for both the neutral and cationic forms.

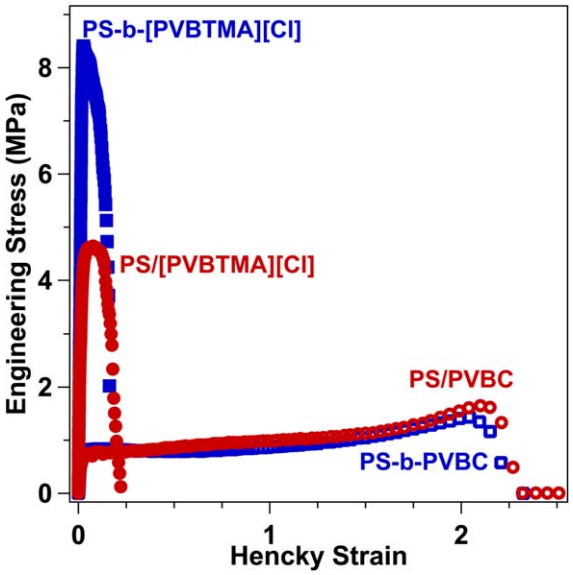

Figure 4. Typical stress vs. strain curve for the four types of films tested: cationic diblock (solid blue), neutral diblock (open blue), cationic blend (solid red), and neutral blend (open red). [Color figure can be viewed in the online issue, which is available at wileyonlinelibrary.com.]

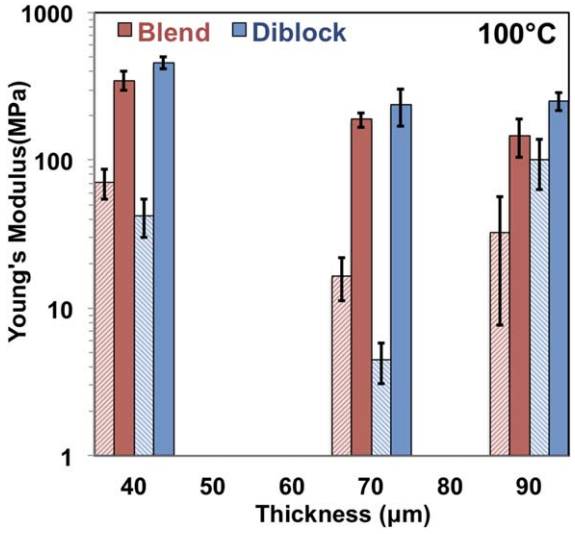

Figure 5. The Young's modulus is displayed for the four polymer chemistries: neutral blend (red dashed), cationic blend (solid red), neutral diblock (dashed blue), cationic diblock (solid blue). [Color figure can be viewed in the online issue, which is available at wileyonlinelibrary.com.]

The Young's modulus, which is the measure of elasticity in the film, increases for all films upon conversion to the cationic form indicating a stiffening of the film with cation addition (Figure 5). The moduli for the films ranged from 4 to 100 MPa for the neutral films and 150 to 450 MPa for the cationic films. Addition of cations to the polymer increases ionic interaction among the polymer chains decreasing elasticity. The moduli did not have an easily defined dependence on film thickness, however the thinnest (40 μm) were slightly stiffer (i.e., larger Young's modulus) in most cases.

The increased stiffness of the cation functionalized films resulted in an increase in stress at break. Stress at failure ranged

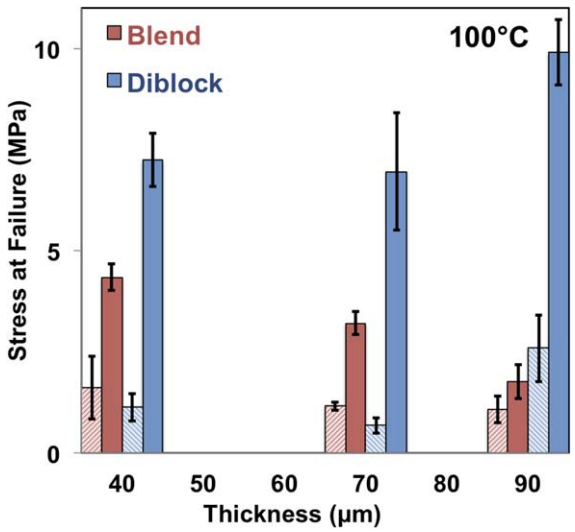

Figure 6. The stress at failure is displayed for the four polymer chemistries: neutral blend (red dashed), cationic blend (solid red), neutral diblock (dashed blue), cationic diblock (solid blue). [Color figure can be viewed in the online issue, which is available at wileyonlinelibrary.com.]

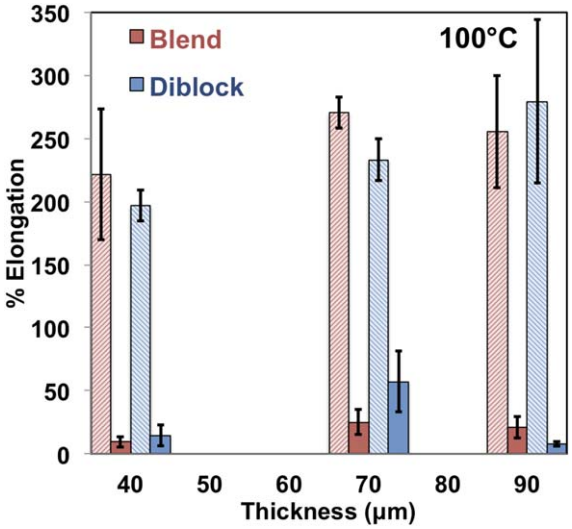

Figure 7. The percent elongation is displayed for the four polymer chemistries: neutral blend (red dashed), cationic blend (solid red), neutral diblock (dashed blue), cationic diblock (solid blue). [Color figure can be viewed in the online issue, which is available at wileyonlinelibrary.com.]

from 0.7 to 2.6 MPa for the neutral films and 1.8–9.9 MPa for the cationic films (Figure 6). The cationic diblock films consistently withstood the highest stress at break, up to 10 MPa, however, this strength is likely too low for sustained use in a fuel cell (e.g., Nafion has a tensile strength 25–43 MPa).[43]

The higher elasticity of the neutral films correlated with significantly larger elongations compared with the cationic forms. Percent elongation ranged from 200 to 280% for the neutral films and only 8–57% for the cationic films (Figure 7). The larger elongations of the neutral films correlate with smaller stresses at break (Figure 6). The low level of elongation in the cationic films would be problematic in a fuel cell where the constrained membrane must be elastic enough to withstand swelling and shrinking that occurs due to humidity changes during operation.

Functionalization of the films with cations caused an increase in stress at failure but severely decreased percent elongation and elasticity. The stiffening of the polymer films when cations are present decreased the mechanical integrity of the films. The loss of mechanical integrity of the polymer film with the addition of

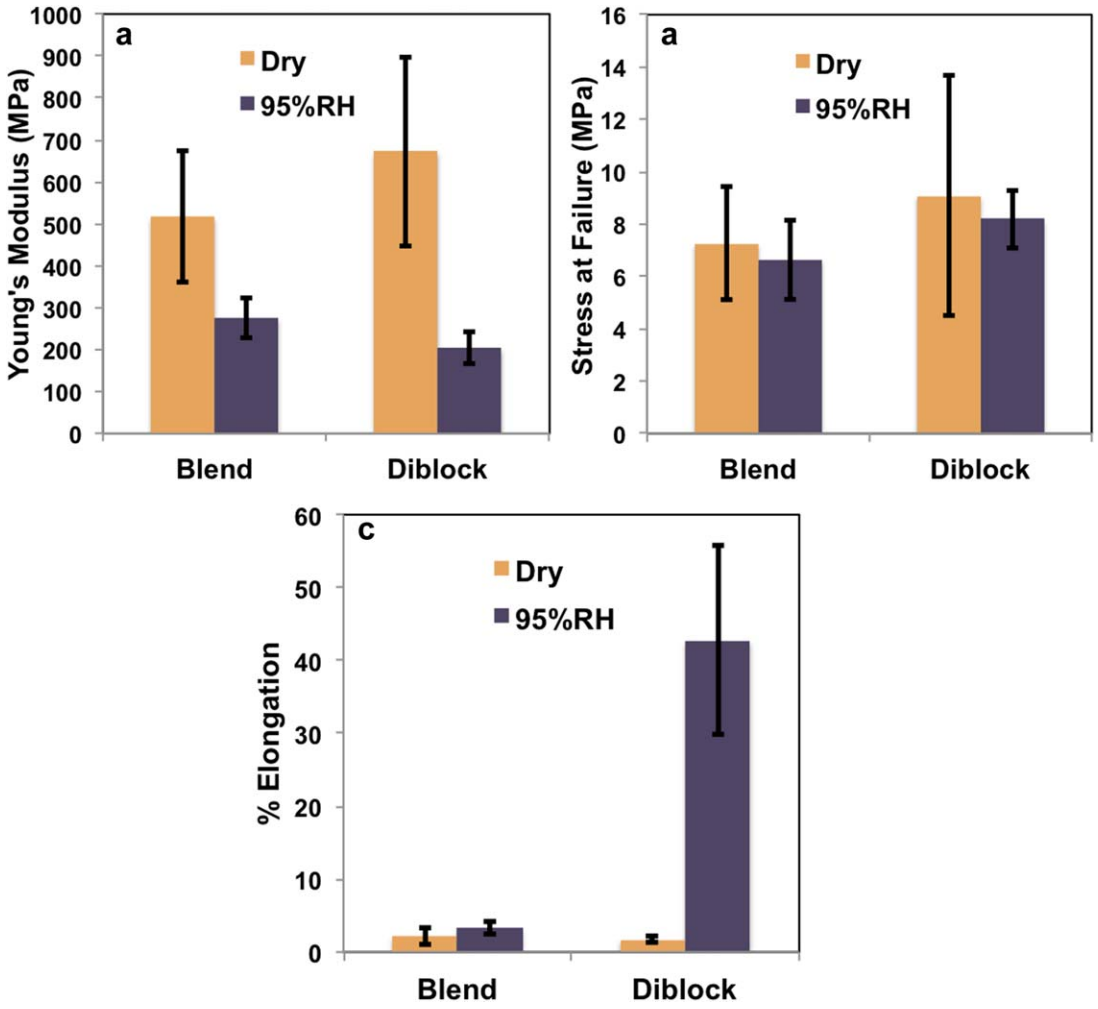

Figure 8. (a) Young's modulus, (b) Stress at failure, and (c) % Elongation for the blend and diblock cationic films at 60°C under dry and humidified conditions. [Color figure can be viewed in the online issue, which is available at wileyonlinelibrary.com.]

cations is discouraging, but highlights the importance of considering mechanical properties when designing AEM polymers.

In addition to the mechanical testing of the films in the neutral and cationic forms at different thicknesses, the cationic films were tested at 60°C under dry and humidified conditions to determine the effect of water sorption on mechanical properties (Figure 8). Films tested at dry and humidified conditions had a nominal thickness of 55 μm. Generally, for ion exchange membranes, water taken up by the polymer acts as a plasticizer, i.e., increasing fluidity, decreasing the modulus and stress, and increasing elongation.[39,44] The Young's modulus for both the diblock and blend films decreased significantly, from between 515 and 625 MPa to between 200 and 275 MPa, when the films were humidified verifying that the plasticizing nature of the water increases film elasticity. Elongation increases significantly for the diblock film, from 2% at dry conditions to 43% at 95%RH. Elongation of the blend films did not change significantly with WU; this could be a result of the low WU of the blend film or the difference in phase separation in the blend. The stress at break for the diblock decreased only slightly, to 8 MPa, from the dry state (9 MPa). The brittleness of the dry polymer films resulted in visible crack formation that contributed to the failure of the membrane in the dry state. Maintaining water in the film reduced crack formation allowing greater elongation of the polymer. The blend membrane showed little difference in stress at break between dry and humidified conditions similar to its elongation behavior, likely due to its low WU. Unfortunately, while the diblock displayed mechanical improvement with water sorption in terms of elongation and elasticity, better mechanical properties are still needed to be comparable with PEMs[6,27,45,46] and other AEMs.[33,39,47]

CONCLUSIONS

The chemical and mechanical properties of a diblock copolymer composed of a hydrophobic, PS block and a hydrophilic, conductive poly(vinylbenzyl trimethylammonium) block were compared with an analogous homopolymer blend. SAXS of the diblock suggested nanoscale size ordering that was dependent on WU by the polymer. Nanoscale features were absent for the homopolymer blend due to the phase separation on the order of 10 μm. The nanometer phase separation of the diblock is favorable for ion conduction, while the micrometer scale phase separation of the homopolymer blend hinders ion conduction. Conductivity of the diblock was comparable with other leading AEMs and was an order of magnitude higher than the homopolymer blend, due to its higher IEC and nanometer scale phase separation. Mechanical integrity of the films was reduced when quaternary ammonium cations were present in the polymer. Percent elongation and elasticity were significantly lower for the cationic polymer films compared with their neutral counterparts. Water taken up by the polymer has a plasticizing effect on the films, increasing elasticity and elongation. The blend films displayed less mechanical response to humidity, likely due to their lower WU. While the nanoscale phase separation of the diblock copolymer produced good ionic conductivity, the high stiffness and low elongation of the films could lead to mechanical failure in an AEM fuel cell. Future work will replace the stiff PS block with a more elastic hydrophobic polymer to improve mechanical properties of the AEM. This study highlights the importance of considering mechanical performance, as well as conductivity, when designing polymers for AEMs.

ACKNOWLEDGMENTS

The authors thank the Army Research Office for support of this research under the MURI #W911NF-10-1-0520 and DURIPs #W911NF-11-1-0306 and #W911NF-11-1-0462. Some measurements were completed as part of the NSF Polymer REU EEC-1156745. Use of the Advanced Photon Source, an Office of Science User Facility operated for the U.S. Department of Energy (DOE) Office of Science by Argonne National Laboratory, was supported by the U.S. DOE under Contract No. DE-AC02-06CH11357.

REFERENCES

1. Steele, B. C.; Heinzel, A. *Nature* **2001**, *414*, 345.
2. Smitha, B.; Sridhar, S.; Khan, A. A. *J. Membr. Sci.* **2005**, *259*, 10.
3. Di Noto, V.; Zawodzinski, T. A.; Herring, A. M.; Giffin, G. A.; Negro, E.; Lavina, S. *Int. J. Hydrogen Ener.* **2012**, *37*, 6120.
4. Couture, G.; Alaaeddine, A.; Boschet, F.; Ameduri, B. *Prog. Polym. Sci.* **2011**, *36*, 1521.
5. McLean, G. F.; Niet, T.; Prince-Richard, S.; Djilali, N. *Int. J Hydrogen Ener.* **2002**, *27*, 507.
6. Borup, R.; Meyers, J.; Pivovar, B.; Kim, Y. S.; Mukundan, R.; Garland, N.; Myers, D.; Wilson, M.; Garzon, F.; Wood, D. *Chem. Rev.* **2007**, *107*, 3904.
7. Hickner, M. A.; Ghassemi, H.; Kim, Y. S.; Einsla, B. R.; McGrath, J. E. *Chem. Rev.* **2004**, *104*, 4587.
8. Varcoe, J. R.; Slade, R. C. T. *Fuel Cells* **2005**, *5*, 187.
9. Merle, G. R.; Wessling, M.; Nijmeijer, K. *J. Membr. Sci.* **2011**, *377*, 1.
10. Kong, X.; Wadhwa, K.; Verkade, J. G.; Schmidt-Rohr, K. *Macromolecules* **2009**, *42*, 1659.
11. Vandiver, M. A.; Horan, J. L.; Yang, Y.; Tansey, E. T.; Seifert, S.; Liberatore, M. W.; Herring, A. M. *J. Polym. Sci. Polym. Phys.* **2013**, *51*, 1761.
12. Hibbs, M. R.; Hickner, M. A.; Alam, T. M.; McIntyre, S. K.; Fujimoto, C. H.; Cornelius, C. J. *Chem. Mater.* **2008**, *20*, 2566.
13. Janarthanan, R.; Horan, J. L.; Caire, B. R.; Ziegler, Z. C.; Yang, Y.; Zuo, X.; Liberatore, M. W.; Hibbs, M. R.; Herring, A. M. *J. Polym. Sci. Polym. Phys.* **2013**, *51*, 1743.
14. Janarthanan, R.; Kishore Pilli, S.; Horan, J. L.; Gamarra, D. A.; Hibbs, M. R.; Herring, A. M. *J. Electrochem. Soc.* **2014**, *161*, F944.
15. Slade, R. C. T.; Varcoe, J. R. *Solid State Ionics* **2005**, *176*, 585.
16. Varcoe, J. R.; Slade, R. C.; Lam How Yee, E.; Poynton, S. D.; Driscoll, D. J.; Apperley, D. C. *Chem. Mater.* **2007**, *19*, 2686.
17. Hickner, M. A.; Herring, A. M.; Coughlin, E. B. *J. Polym. Sci. Polym. Phys.* **2013**, *51*, 1727.

18. Hayes, W. M. CRC Handbook of Chemistry and Physics; CRC Press, Inc., **2011**; 92nd ed.
19. Bates, F. S.; Fredrickson, G. H. *Phys. Today* **1999**, *52*, 32.
20. Gadjourova, Z.; Andreev, Y. G.; Tunstall, D. P.; Bruce, P. G. *Nature* **2001**, *412*, 520.
21. Bates, F. S. *Science* **1991**, *251*, 898.
22. Tsai, T.-H.; Maes, A. M.; Vandiver, M. A.; Versek, C.; Seifert, S.; Tuominen, M.; Liberatore, M. W.; Herring, A. M.; Coughlin, E. B. *J. Polym. Sci. Polym. Phys.* **2012**, *51*, 1751.
23. Sudre, G.; Inceoglu, S.; Cotanda, P.; Balsara, N. P. *Macromolecules* **2013**, *46*, 1519.
24. Li, Y. Block Copolymer for Alkaline Fuel Cell Membrane Materials; Colorado School of Mines: Golden, CO, **2014**, p 1.
25. Neburchilov, V.; Martin, J.; Wang, H.; Zhang, J. *J. Power Sources* **2007**, *169*, 221.
26. Patil, Y. P.; Jarrett, W. L.; Mauritz, K. A. *J. Membr. Sci.* **2010**, *356*, 7.
27. Tang, Y.; Karlsson, A. M.; Santare, M. H.; Gilbert, M.; Cleghorn, S.; Johnson, W. B. *Mater. Sci. Eng.: A* **2006**, *425*, 297.
28. Lai, Y.-H.; Mittelsteadt, C. K.; Gittleman, C. S.; Dillard, D. A. *J. Fuel Cell Sci. Technol.* **2009**, *6*, 021002.
29. Dillard, D. A.; Li, Y.; Grohs, J. R.; Case, S. W.; Ellis, M. W.; Lai, Y.-H.; Budinski, M. K.; Gittleman, C. S. *J. Fuel Cell Sci. Technol.* **2009**, *6*, 031014.
30. Schlichting, G. J.; Horan, J. L.; Jessop, J. D.; Nelson, S. E.; Seifert, S.; Yang, Y.; Herring, A. M. *Macromolecules* **2012**, *45*, 3874.
31. Liu, Y.; Horan, J. L.; Schlichting, G. J.; Caire, B. R.; Liberatore, M. W.; Hamrock, S. J.; Haugen, G. M.; Yandrasits, M. A.; Seifert, S.; Herring, A. M. *Macromolecules* **2012**, 120911063431009.
32. Sentmanat, M. L. *Rheol. Acta* **2004**, *43*, 657.
33. Vandiver, M. A.; Caire, B. R.; Carver, J. R.; Waldrop, K.; Hibbs, M. R.; Varcoe, J. R.; Herring, A. M.; Liberatore, M. W. *J. Electrochem. Soc.* **2014**, *161*, H677.
34. Zawodinski, T. A. J.; Springer, T. E.; Davey, J.; Jestel, R.; Lopez, C.; Valerio, J.; Gottesfield, S. *J. Electrochem. Soc.* **1993**, *140*, 1981.
35. Burnett, D. J.; Garcia, A. R.; Thielmann, F. *J. Power Sources* **2006**, *160*, 426.
36. Park, M. J.; Downing, K. H.; Jackson, A.; Gomez, E. D.; Minor, A. M.; Cookson, D.; Weber, A. Z.; Balsara, N. P. *Nano Lett.* **2007**, *7*, 3547.
37. Li, Y. S.; Zhao, T. S.; Yang, W. W. *Int. J. Hydrogen Ener.* **2010**, *35*, 5656.
38. Lin, X.; Wu, L.; Liu, Y.; Ong, A. L.; Poynton, S. D.; Varcoe, J. R.; Xu, T. *J. Power Sources* **2012**, *217*, 373.
39. Fujimoto, C.; Kim, D.-S.; Hibbs, M.; Wrobleski, D.; Kim, Y. S. *J. Membr. Sci.* **2012**, *423*, 438.
40. Wang, J.; Li, S.; Zhang, S. *Macromolecules* **2010**, *43*, 3890.
41. Yan, J.; Hickner, M. A. *Macromolecules* **2010**, *43*, 2349.
42. Halseid, R.; Vie, P. J. S.; Tunold, R. *J. Electrochem. Soc.* **2004**, *151*, A381.
43. DuPont. *DuPont Nafion PFSA Membranes*; data sheet, **2009**; p 1.
44. Silberstein, M. N.; Boyce, M. C. *J. Power Sources* **2010**, *195*, 5692.
45. Sgreccia, E.; Chailan, J. F.; Khadhraoui, M.; Di Vona, M. L.; Knauth, P. *J. Power Sources* **2010**, *195*, 7770.
46. Satterfield, M. B.; Benziger, J. B. *J. Polym. Sci. Polym. Phys.* **2009**, *47*, 11.
47. Robertson, N. J.; Kostalik, H. A., IV; Clark, T. J.; Mutolo, P. F.; Abruña, H. D.; Coates, G. W. *J. Am. Chem. Soc.* **2010**, *132*, 3400.